Journal of Solid State Chemistry **154,** 524–529 (2000)
doi:10.1006/jssc.2000.8873, available online at http://www.idealibrary.com on IDEAL®

Structural Phase Transition of Orthorhombic $LaCrO_3$ Studied by Neutron Powder Diffraction

K. Oikawa,[1] T. Kamiyama,* T. Hashimoto,† Y. Shimojyo, and Y. Morii

*Advanced Science Research Center, Japan Atomic Energy Research Institute, Tokai, Ibaraki 319-1195, Japan; *Institute of Materials Science, University of Tsukuba, Tennodai, Tsukuba, Ibaraki 305-8573, Japan; and †Department of Applied Physics, College of Humanities and Sciences, Nihon University, Setagaya-ku, Tokyo 156-8550, Japan*

Received October 28, 1999; in revised form June 6, 2000; accepted July 17, 2000; published online September 30, 2000

An orthorhombic to a rhombohedral structural phase transition of $LaCrO_3$ has been studied by the neutron powder diffraction over the temperature range of 295–1013 K. At the phase transition around 260°C, the negative volume expansion was observed, and the amount of the volume compression was estimated to be -0.081375 Å^3 (-0.138%) per formula unit. The coefficients of volume thermal expansion, $-(1/V)/(\partial V/\partial T)$, were estimated to be $2.285(16)\times10^{-5}$ K^{-1} and $2.842(12)\times10^{-5}$ K^{-1} for the orthorhombic and rhombohedral phases, respectively. The Rietveld refinement revealed that the volume compression at the phase transition was principally due to the shrinking of the $[CrO_6]$ octahedra. © 2000 Academic Press

Key Words: **lanthanum chromite; structural phase transition; neutron powder diffraction; Rietveld refinement.**

INTRODUCTION

$LaCrO_3$ and related oxides have been studied widely, focusing on various industrial uses above room temperature (RT): for example, interconnects in solid–oxide fuel cells (1, 2). It is well known that stoichiometric $LaCrO_3$ has phase transitions at around $T = 15$ and 260°C. The former is due to a magnetic order–disorder transition, while the latter is due to a structural phase transition, i.e., from an orthorhombic to a rhombohedral symmetry (3–10). The structural phase transition to a cubic symmetry was suggested to occur above 1600°C (3, 4, 7), but it is not fully understood because of its experimental difficulty. Although the physical properties such as heat capacity and thermal conductivity of $LaCrO_3$–based perovskites at high temperatures have been measured widely (11–14), the crystal structure above room temperature has not been examined precisely.

Howard *et al.* (6) studied an orthorhombic to a rhombohedral structural phase transition of the $La(Cr_{1-x}Mn_x)O_3$ ($x = 0$ to 0.25) system by X-ray powder diffraction. The phase transition temperatures as a function of Mn contents were determined by individual profile fitting in a 2θ range of 31.0°–33.0°. The decrease in the unit cell volume of $LaCrO_3$ at the phase transition around 265°C was found to be about -0.2%. Gilbu *et al.* (8) studied structural phase transition of the $La(Co_{1-t}Cr_t)O_3$ ($t = 0$ to 1.0) system by X-ray powder diffraction. The phase transition temperature increases with t, while the volume contraction at the structural phase transition decreases: $0.25(7)\times10^6$ pm^3 (-0.43%), $0.13(7)\times10^6$ pm^3 (-0.22%), and $0.10(5)\times10^6$ pm^3 (-0.17%) per formula unit for $t = 0.80$, 0.90, and 1.00, respectively. Sakai *et al.* (9) studied structural phase transition of the $(La_{1-t}Ca_t)CrO_{3-\delta}$ ($t = 0$ to 0.3) system by X-ray powder diffraction. The volume contraction at the structural phase transition was -0.14% and -0.07% for $t = 0$ and 0.20, respectively. In addition to the thermally induced phase transition, Hashimoto *et al.* (10) found a structural phase transition under high pressure at RT using synchrotron X-ray powder diffraction. They discussed the thermodynamic relation between the pressure and the temperature of the phase transition.

It remains open whether the large volume contraction arises from the deformation of $[LaO_{12}]$ and/or $[CrO_6]$ polyhedra. Then we carried out neutron diffraction experiments on $LaCrO_3$ at several temperatures between 22 and 740°C on warming and studied the structural phase transition from an orthorhombic to a rhombohedral phase. A geometrical relationship between polyhedral volumes and their tilts in perovskites developed by Thomas (15–17) was utilized to deduce polyhedral volume changes at the phase transition.

[1]Present address: National Institute of Materials and Chemical Research, Agency of Industrial Science and Technology, 1-1 Higashi, Tsukuba, Ibaraki 305-8565, Japan. Fax: +81-298-61-4541. E-mail: oikawa@nimc.go.jp.

0022-4596/00 $35.00

EXPERIMENTAL

A powder specimen was prepared from polycrystalline $LaCrO_3$ (99%, Nikkato Co., Ltd.) annealed at 1300°C for 24 h in O_2 atmosphere.

Neutron powder diffraction data were taken on HRPD at the JRR-3 in Japan Atomic Energy Research Institute. Two different wavelengths were selected depending on the requirement for the present study. The elastically bent Si (533) monochromator, which gives wavelength of 1.16251 Å (18), was mainly used to obtain detailed structural information for the orthorhombic phase including anisotropic displacement parameters because of their wide Q range ($0.5\ Å^{-1} < Q < 10.7\ Å^{-1}$). The hot-pressed Ge (331) monochromator which gives 1.82340 Å was employed at around the phase transition region in order to obtain higher Q-resolution and at a high temperature region. Soller slit collimators of 12′ and 20′ were positioned before and after the monochromator, respectively. An array of 64 nearly equally spaced (2.5°) ^{3}He detectors with 6′ Soller collimators were used to collect the intensity data between 5° and 165° with a step width of 0.05°. A counting time for each step was 800 s (Si monochromator) and 300 s (Ge monochromator). The sample contained in a cylindrical V can (16.5 mm in diameter, 50 mm in height and 0.5 mm in thickness) was mounted on an evacuated high-temperature furnace. The temperature was monitored by a Chromel-Alumel thermocouple and was kept within ± 0.5 K during the measurement. A waiting time for ensuring the equilibrium of the sample temperature was about 0.5 h.

RESULTS AND DISCUSSION

Neutron diffraction data for scattering angles between 12.5° and 162.5° were analyzed by a Rietveld-refinement program RIETAN (19). Coherent scattering lengths used for the refinements of the neutron data were 8.24 (La), 3.635 (Cr), and 5.803 fm (O) (20). The pseudo-Voigt function of Thomson, Cox, and Hastings (21) was made asymmetric with Howard's procedure (22). In final refinements, a zero-point error, a Gaussian FWHM parameter, U, and a Lorentzian FWHM parameter, X, were varied, while Gaussian FWHM parameters, V and W, a Lorentzian FWHM parameter, Y, and an asymmetric parameter, A, were fixed to the average values obtained from preliminary refinements. Preferred orientation was examined using March-Dollase function in the preliminary refinements. Since the resultant value of a preferred-orientation parameter was close to unity, preferred orientation was not corrected in the final refinement.

The transition temperature was estimated to be 260°C, where coexistence of orthorhombic and rhombohedral phases was revealed by the Rietveld refinement. The diffraction data below this temperature were analyzed on the basis of orthorhombic space group *Pnma* (No. 62, $a \sim 5.5$ Å, $b \sim 7.8$ Å, and $c \sim 5.5$ Å) (23). On the other hand, the crystal structure of $LaCrO_3$ at rhombohedral phase has not been reported before. Only the lattice parameters and/or possible space groups were indicated by several workers. In the Rietveld refinement of the rhombohedral phase, we tested structural models based on the space groups $R\bar{3}$, $R\bar{3}m$, and $R\bar{3}c$. The $R\bar{3}m$ model was easily rejected by the strong additional reflections due to doubling of the c axis. The refinements based on the $R\bar{3}c$ model and the $R\bar{3}$ model gave almost the same structural parameters and R values, but the estimated standard deviations (e.s.d.s) were very large for the $R\bar{3}$ model. The extinction rules of $R\bar{3}c$ were fully consistent with the observations. These preliminary refinements led us to rule out $R\bar{3}$ and adopt $R\bar{3}c$ in final refinements. The choice of the space group $R\bar{3}c$ was also supported by the study using the convergent beam electron diffraction (24). The structure in $R\bar{3}c$ is a common high temperature form in $LaVO_3$, $LaMnO_3$, and $LaFeO_3$, as well as in the $LaCoO_3$ and $LaNiO_3$ at all temperatures.

Examples of refined structural parameters, selected bond distances, and angles for the orthorhombic phase (200°C) and the rhombohedral phase (320°C) with a wavelength of 1.16251 Å were summarized in Table 1 and their Reitveld-refinement patterns are given in Figs. 1a and 1b. Typical R_{wp} and R_B were ca. 7 and 3%, respectively. Figure 2 shows the volume per formula unit as a function of temperature. The

TABLE 1
Structure Parameters of $LaCrO_3$ at 200°C (Orthorhombic Phase) and 320°C (Rhombohedral Phase) Obtained by the Rietveld Refinements

$T = 200$°C	*Pnma* (No. 62)	$T = 320$°C	$R\bar{3}c$ (No. 167)
R_{wp}	7.14%	R_{wp}	7.41%
R_B	3.07%	R_B	3.01%
S	1.151	S	1.163
a	5.48588(14)	a	5.53049(11)
b	7.76824(19)		
c	5.52467(12)	c	13.3544(3)
V	235.437(10)	V	353.738(12)
La		La	
x	0.0167(5)	x	0
y	$\frac{1}{4}$	y	0
z	−0.0037(5)	z	$\frac{1}{4}$
U_{11}	0.0063(11)	U_{11}	0.0084(7)
U_{22}	0.0086(11)	U_{22}	0.0084
U_{33}	0.0051(8)	U_{33}	0.0089(13)
U_{12}	0	U_{12}	0.0042
U_{13}	0.0010(9)	U_{13}	0
U_{23}	0	U_{23}	0
B_{eq}	0.53(14)	B_{eq}	0.68(19)
Cr		Cr	
x	0	x	0
y	0	y	0
z	$\frac{1}{2}$	z	0
U_{11}	—	U_{11}	0.0038(12)

TABLE 1—*Continued*

$T = 200°C$	*Pnma* (No. 62)	$T = 320°C$	$R\bar{3}c$ (No. 167)
U_{22}	—	U_{22}	0.0038
U_{33}	—	U_{33}	0.0063(23)
U_{12}	—	U_{12}	0.0019
U_{13}	—	U_{13}	0
U_{23}	—	U_{23}	0
B_{eq}	—	B_{eq}	0.37(25)
B	0.27(4)*		
O1		O	
x	0.4935(8)	x	0.4935(8)
y	$\frac{1}{4}$	y	0
z	0.0646(6)	z	$\frac{1}{4}$
U_{11}	0.0118(19)	U_{11}	0.0120(6)
U_{22}	0.0038(15)	U_{22}	0.0097(9)
U_{33}	0.0083(11)	U_{33}	0.0150(9)
U_{12}	0	U_{12}	0.0049
U_{13}	−0.0001(14)	U_{13}	−0.0039(5)
U_{23}	0	U_{23}	−0.0060
B_{eq}	0.63(17)	B_{eq}	0.99(16)
O2			
x	0.2282(5)		
y	0.5350(3)		
z	0.2285(5)		
U_{11}	0.0085(10)		
U_{22}	0.0113(10)		
U_{33}	0.0071(9)		
U_{12}	0.0008(10)		
U_{13}	0.0036(9)		
U_{23}	0.0005(10)		
B_{eq}	0.71(15)		
La–O1^{i}	2.429(4)	La–O × 3	2.4564(19)
La–O2^{ii} × 2	2.478(3)		
La–O2^{iii} × 2	2.635(4)	La–O^{xi} × 6	2.7565(2)
La–O1	2.643(5)		
La–O2 × 2	2.809(3)		
La–O1^{iv}	2.895(5)		
La–O1^{v}	3.102(4)	La–O2^{xii} × 3	3.0741(19)
La–O2^{i} × 2	3.117(3)		
$\overline{\text{La–O}}$	2.7620	$\overline{\text{La–O}}$	2.7609
Cr–O2^{vi} × 2	1.973(3)	Cr–O^{xi} × 6	1.9705(3)
Cr–O2^{vii} × 2	1.973(3)		
Cr–O1^{viii} × 2	1.9749(6)		
$\overline{\text{Cr–O}}$	1.9733	$\overline{\text{Cr–O}}$	1.9705
O1^{viii}–Cr–O2^{vii}	89.67(14)	O^{xiii}–Cr–O^{xi} × 3	88.766(9)
O1^{viii}–Cr–O2^{vi}	89.46(15)		
O2^{vii}–Cr–O2^{vi}	88.52(2)		
Cr^{ix}–O1–Cr^{x}	159.07(19)	Cr^{xiv}–O–Cr^{xv}	161.97(11)
Cr^{vi}–O2–Cr^{x}	161.36(14)		
		O^{xvi}–O–O^{xvii}	141.90(13)

Note. U_{ij}s are anisotropic displacement parameters when the displacement factor is expressed as $\exp[-2\pi^2(U_{11}(ha^*)^2 + \cdots + 2U_{12}ha^*kb^* + \cdots)]$. B_{eq} is the equivalent isotropic displacement parameter. Numbers in parentheses following refined parameters represent the e.s.d.s of the last significant digit(s).

Symmetry codes: i, $-\frac{1}{2}+x, y, \frac{1}{2}-z$, ii, $-x, -\frac{1}{2}+y, -z$; iii, $\frac{1}{2}-x, 1-y, -\frac{1}{2}+z$, iv, $-1+x, y, z$; v, $-\frac{1}{2}+x, y, -\frac{1}{2}-z$; vi, $x, \frac{1}{2}-y, z$; vii, $-\frac{1}{2}+x, \frac{1}{2}-y, \frac{1}{2}-z$; viii, $\frac{1}{2}-x, -y, \frac{1}{2}+z$; ix, $\frac{1}{2}+x, y, \frac{1}{2}-z$; x, $\frac{1}{2}+x, \frac{1}{2}-y, \frac{1}{2}-z$; xi, $\frac{2}{3}-x, \frac{1}{3}-y, \frac{1}{3}-z$; xii, $-1+x, y, z$; xiii, $\frac{1}{3}-x+y, \frac{2}{3}-x, -\frac{1}{3}+z$; xiv, $\frac{2}{3}+x, \frac{1}{3}+y, \frac{1}{3}+z$; xv, $\frac{1}{3}-y, -\frac{1}{3}-x, \frac{1}{8}+z$; xvi, $-y, -1+x-y, z$; xvii, $1-x+y, 1-x, z$.

[a]Anisotropic atomic displacement parameters were not refined.

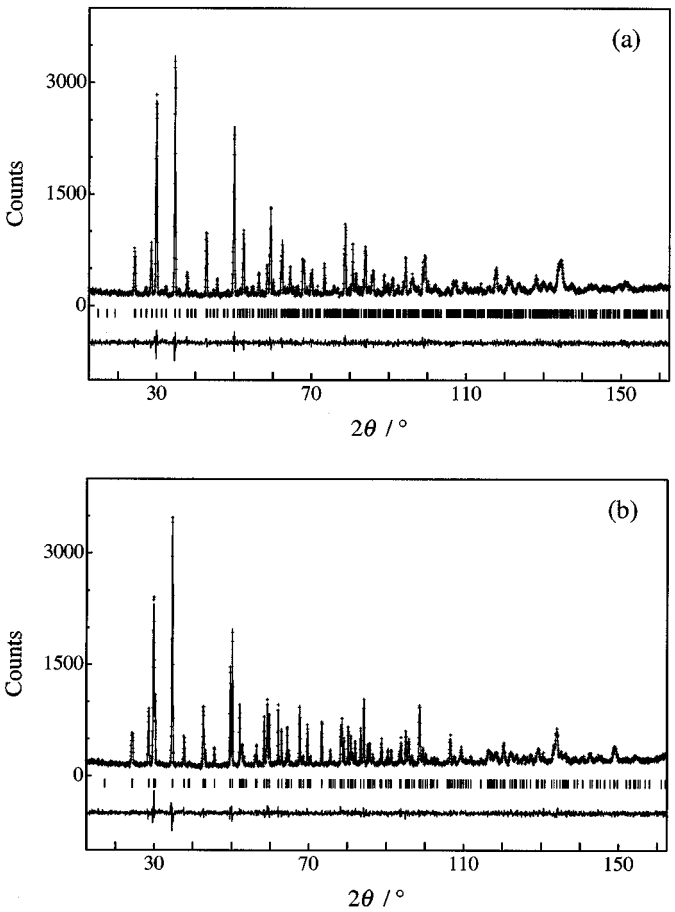

FIG. 1. Rietveld refinement patterns of $LaCrO_3$ at (a) 200°C (orthorhombic phase) and (b) 320°C (rhombohedral phase). Observed intensity data are shown by crosses, and the solid line overlying them is the calculated intensity. Vertical markers below the diffraction patterns indicate positions of possible Bragg reflections. Differences between the observed and calculated intensities are plotted at the bottom in the same scale.

coefficients of volume thermal expansion, $-(1/V)/(\partial V/\partial T)$, were estimated from least-squares analysis as $2.285(16)\times10^{-5}\,K^{-1}$ (between $T = 295$ K and $T = 533$ K) and $2.842(12)\times10^{-5}\,K^{-1}$ (between $T = 533$ K and $T = 1013$ K) for the orthorhombic and rhombohedral phases, respectively. The volume contraction at the phase transition was calculated to be about −0.138%, which is very close to the values reported by Sakai *et al.* (9).

As shown in Fig. 3 , average bond distances in $[LaO_{12}]$ and $[CrO_6]$ polyhedra, $\overline{\text{La–O}}$ and $\overline{\text{Cr–O}}$, and their ratio, $(1/\sqrt{2})/(\overline{\text{La–O}}/\overline{\text{Cr–O}})$, vary discontinuously at the phase transition, but the slope of the ratio is almost the same in the whole temperature range. The ratio indicates size mismatch between two polyhedra at LaO and CrO_2 layers, and the discontinuity might not be explained by the simple rotation of $[CrO_6]$ octahedra. Then we examined the polyhedral volumes as shown below.

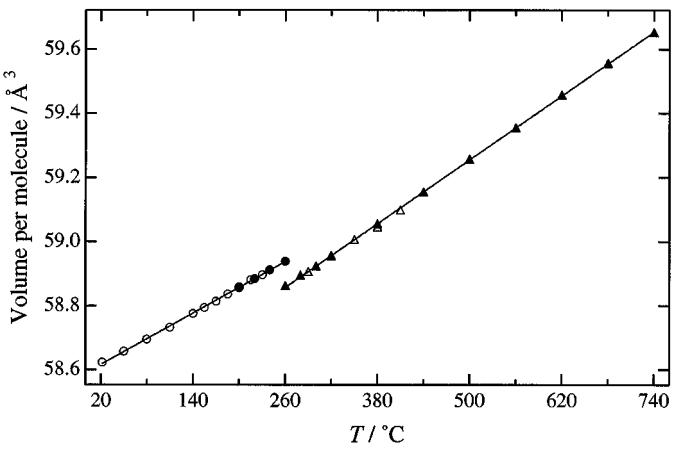

FIG. 2. Dependence of the volume per formula unit of the $LaCrO_3$ on temperature, T. Circles and triangles express the volume for the orthorhombic and the rhombohedral phases, respectively. Data points obtained from experiments with wavelength of 1.82340 Å are represented by filled symbols.

The relationship between polyhedral volumes and their shapes in orthorhombic and rhombohedral perovskites ABO_3 were discussed by Thomas *et al.* (15–17). For orthorhombic perovskites, the volume of the $[AO_{12}]$ polyhedron, V_A, that of the $[BO_6]$ polyhedron, V_B, and their ratio V_A/V_B are given by

$$V_B = \frac{s_1 s_2 s_3}{6},$$

$$\frac{V_A}{V_B} = 6\cos^2\theta_m \cos\theta_z - 1,$$

where s_1, s_2, and s_3 are distances between diagonal vertices of an octahedron, and θ_m and θ_z the tilt angles of the $[BO_6]$ octahedra along [101] and [010] direction of the present setting, respectively. To derive more accurate volumes of the $[BO_6]$ octahedra, deviations of the $O2^{iii}$–Cr–$O2^{v}$ angle from a right angle are considered in the present study, while the $O1^{viii}$–Cr–$O2^{vii}$ and $O1^{viii}$–Cr–$O2^{vi}$ angles are regarded as a right angle.

For rhombohedral perovskites, V_A, V_B, V_A/V_B, and octahedral tilt angle, ω, are given by

$$V_B = \frac{\sqrt{3}cs^2}{18},$$

$$V_A = \frac{\sqrt{3}a^2c}{12} - \frac{\sqrt{3}cs^2}{18},$$

$$\cos\omega = \frac{a}{2s},$$

and

$$\frac{V_A}{V_B} = 6\cos^2\omega - 1,$$

where a and c are the lattice constants in the hexagonal unit cell, and s the edge length of the $[BO_6]$ octahedra. From these equations given by Thomas *et al.*, V_A, V_B, and V_A/V_B for both the orthorhombic and the rhombohedral phases were calculated and plotted in Fig. 4. We can clearly see the shrinking of V_B at the phase transition and almost linear expansion of V_A at whole temperature range. This figure unambiguously reveals that the volume contraction at the phase transition principally results from the shrinking of the $[BO_6]$ polyhedron.

Thomas introduced a parameter Φ to combine θ_m and θ_z in orthorhombic structure:

$$\Phi = 1 - \cos^2\theta_m \cos\theta_z.$$

Using Φ, V_A/V_B can be simply written as

$$\frac{V_A}{V_B} = 5 - 6\Phi.$$

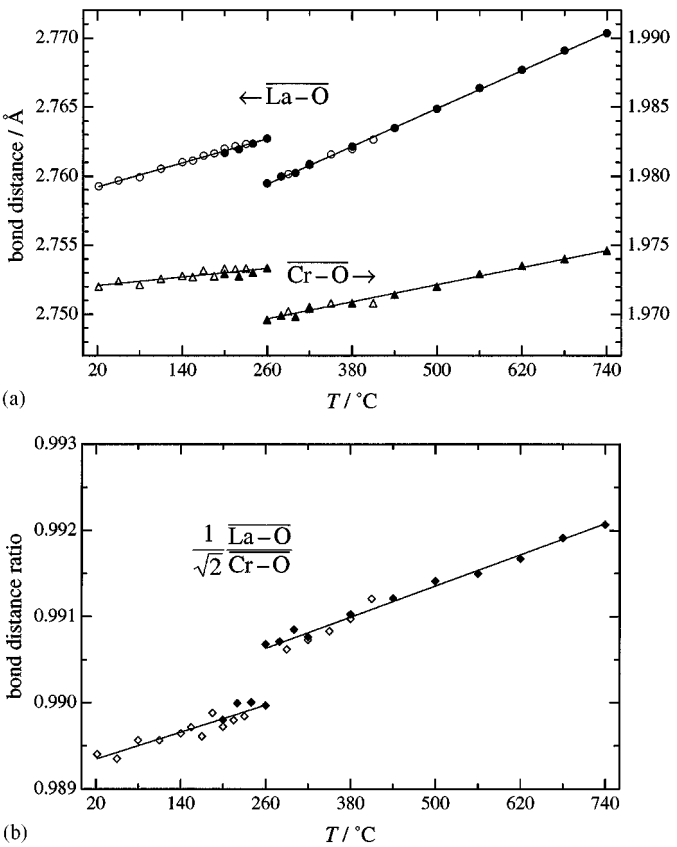

FIG. 3. Average bond distances, $\overline{La–O}$ and $\overline{Cr–O}$ (a), and their ratio, $(1/\sqrt{2})/(\overline{La–O}/\overline{Cr–O})$ (b), of the $LaCrO_3$ as a function of T.

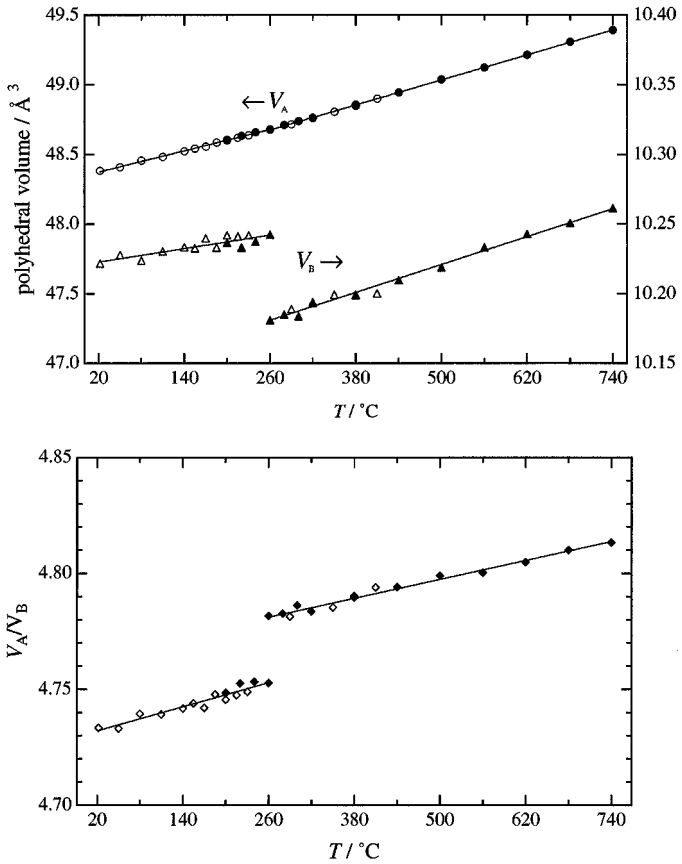

FIG. 4. Temperature variation of the volume of the $[LaO_{12}]$ polyhedron, V_A, and of the $[CrO_6]$ polyhedron, V_B (a), and their ratio V_A/V_B (b) of the $LaCrO_3$.

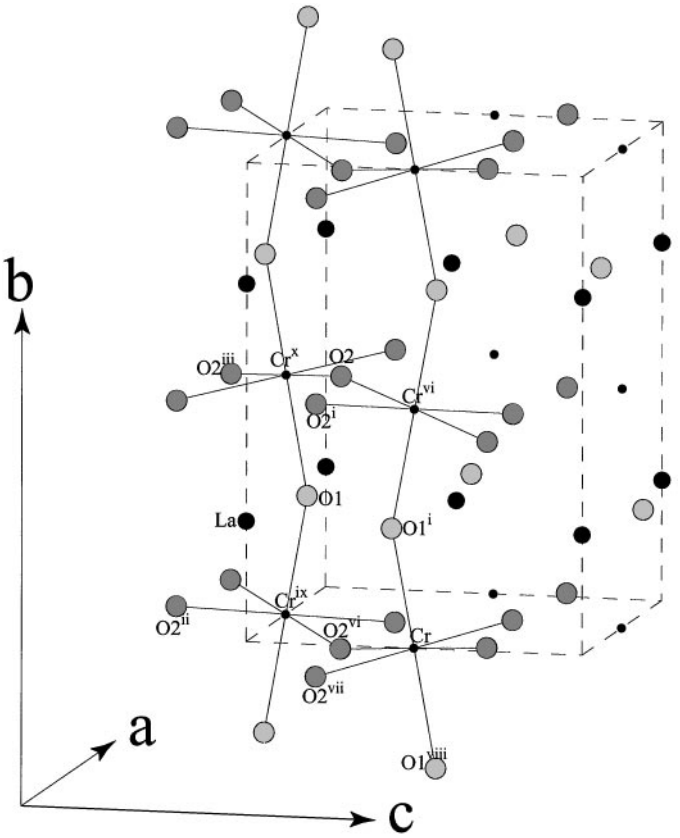

FIG. 5. Crystal structure of $LaCrO_3$ for orthorhombic phase. Large black, small black, and large gray circles represent La, Cr, O, atoms, respectively. Symmetry codes are the same as those in the Table 1.

In order to extend Φ to the rhombohedral structure and to study the characteristics of the phase transition in the present system, the degree of tilt in rhombohedral structure is expressed as

$$\Phi = 1 - \cos^2 \omega.$$

Using Φ, V_A/V_B is similarly written as

$$\frac{V_A}{V_B} = 5 - 6\Phi.$$

V_A/V_B of both orthorhombic and rhombohedral phases in $LaCrO_3$ is plotted as a function of Φ in Fig. 7. V_A/V_B of various known samples (15, 16, 25–29) having orthorhombic (space group *Pnma*) and rhombohedral (space group $R\bar{3}c$) structure are also included in the figure. The rhombohedral samples tend to have smaller tilts Φ and larger V_A/V_B values. It is emphasized in the case of $LaCrO_3$ that Φ decreases as the phase transition from the orthorhombic to rhombohedral proceeds, and its phase boundary is

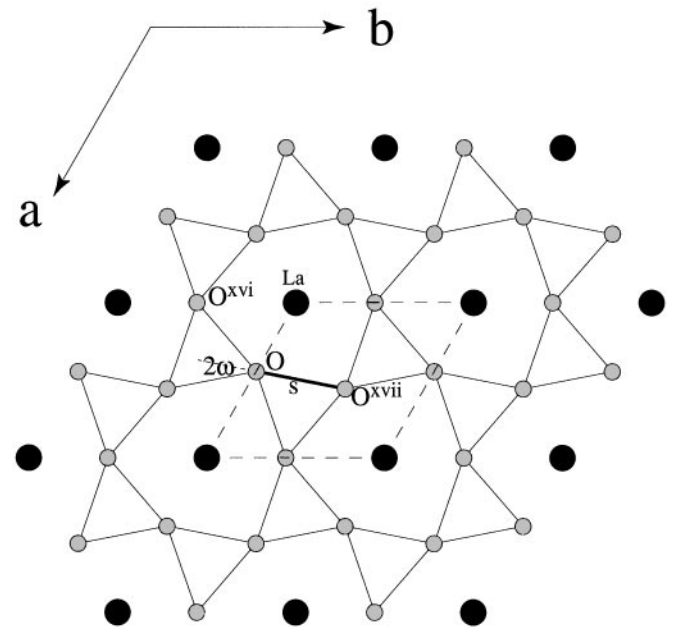

FIG. 6. A plane view of $LaCrO_3$ for rhombohedral phase seen from c axis of hexagonal cell in $z = 14$. Large black and large gray circles represent La and O atoms, respectively. Symmetry codes are the same with the Table 1.

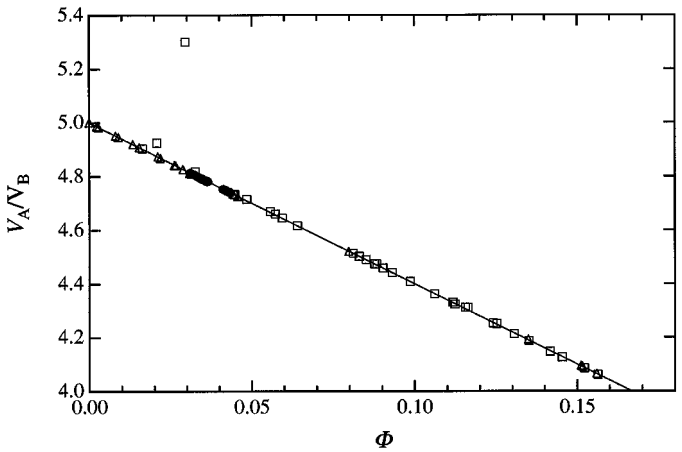

FIG. 7. Variation of V_A/V_B of $LaCrO_3$ with degree of tilt Φ (circles). Triangles and squares represent that of rhombohedral (space group $R\bar{3}c$) and orthorhombic (space group *Pnma*) perovskites.

located near the limit of the reference values of rhombohedral samples.

It is curious that the $[BO_6]$ polyhedron contracts instead of the $[AO_{12}]$ polyhedron, because the V_B is much tighter than V_A. The same kind of contraction would occur in the structural phase transition of $La(Co_{1-t}Cr_t)O_3$, $(La_{1-t}A_t)CrO_3$ (A = Ca or Sr) system. Further investigations are required to clarify the origin of the V_B contraction.

REFERENCES

1. H. Yokokawa, N. Sakai, T. Kawada, and M. Dokiya, *J. Electrochem. Sci.* **138,** 1018 (1991).
2. N. Q. Minh, *J. Am. Ceram. Soc.* **76,** 563 (1993).
3. J. S. Ruiz, A. M. Anthony, and M. Foex, *C.R. Acad. Sci. Paris B* **264,** 1271 (1967).
4. S. Geller and P. M. Raccah, *Phys. Rev. B* **2,** 1167 (1970).
5. A. C. Momin, E. B. Mirza, and M. D. Mathews, *J. Mater. Sci. Lett.* **10,** 1246 (1991).
6. S. A. Howard, J. Yau, and H. U. Anderson, *J. Am. Ceram. Soc.* **75,** 1685 (1991).
7. H. E. Höfer and W. F. Kock, *J. Electrochem. Soc.* **140,** 2889 (1993).
8. B. Gilbu, H. Fjellvag, and A. Kjekshus, *Acta Chem. Scand.* **48,** 37 (1994).
9. N. Sakai, H. Fjellvag, and B. C. Hauback, *J. Solid State Chem.* **121,** 202 (1996).
10. T. Hashimoto, N. Matsushita, Y. Murakami, N. Kojima, K. Yoshida, H. Tagawa, M. Dokiya, and T. Kikegawa, *Solid State Commun.* **108,** 691 (1998).
11. B. Gilbu Tilset, H. Fjellvag, and A. Kjekshus, *J. Solid State Chem.* **119,** 271 (1995).
12. N. Sakai and S. Stolen, *J. Chem. Thermodyn.* **27,** 493 (1995).
13. H. Satoh, S. Koseki, M. Takagi, W. Y. Chung, and N. Kamegashira, *J. Alloys Compd.* **259,** 176 (1997).
14. T. Nakamura, G. Petzow, and L. J. Gauckler, *Mater. Res. Bull.* **14,** 649 (1979).
15. N. W. Thomas and A. Beitollahi, *Acta Crystallogr. B* **50,** 549 (1994).
16. N. W. Thomas, *Acta Crystallogr. B* **52,** 16 (1996).
17. N. W. Thomas, *Acta Crystallogr. B* **52,** 954 (1996).
18. I. Tanaka, N. Nimura, and P. Mikula, *J. Appl. Crystallogr.* **32,** 525 (1999).
19. Y.-I. Kim and F. Izumi, *J. Ceram. Soc. Jpn.* **102,** 401 (1996).
20. V. F. Sears, *in* "International Tables for Crystallography" (A. J. C. Wilson, Ed.), Vol. C, pp. 383–391. Kluwer Academic, Dordrecht, 1992.
21. P. Thompson, D. E. Cox, and J. B. Hastings, *J. Appl. Crystallogr.* **20,** 79 (1987).
22. C. J. Howard, *J. Appl. Crystallogr.* **15,** 615 (1982).
23. C. P. Khattak and D. E. Cox, *Mater. Res. Bull.* **12,** 463 (1977).
24. T. Hashimoto, K. Takagi, K. Tsuda, M. Tanaka, K. Yoshida, H. Tagawa, and M. Dokiya, *in* "Proceedings of the 6th International Symposium of Solid Oxide Fuel Cells," The Electrochemical Society Proceedings, Vol. 99-19, p. 649 (1999).
25. J. L. Garcia-Munoz, Rodriguez-Carvajal, P. Lacorre, and J. B. Torrance, *Phys. Rev. B* **46,** 4414 (1992).
26. S. E. Dann, D. B. Currie, M. T. Weller, M. F. Thomas, and A. D. Al Rawwas, *J. Solid State Chem.* **109,** 134 (1994).
27. H. Falcon, A. E. Goeta, G. Punte, and R. E. Carbonio, *J. Solid State Chem.* **133,** 379 (1997).
28. W. Marti, P. Fischer, J. Schefer, and F. Kubel, *Z. Kristallogr.* **211,** 891 (1996).
29. B. C. Chakoumakos, D. G. Schlom, M. Urbanik, and J. Luine, *J. Appl. Phys.* **83,** 1979 (1998).